Reconstruction of electron spectra using singular component decomposition

Alexei V. Chvetsov
Department of Medical Physics, Tom Baker Cancer Centre, 1331 29th Street N.W., Alberta T2N 4N2, Canada

George A. Sandison
School of Health Sciences, Purdue University, West Lafayette, Indiana 47907

(Received 8 August 2001; accepted for publication 25 January 2002; published 21 March 2002)

Reconstruction of electron spectra of medical accelerators from measured depth dose distributions is an attractive tool for commissioning of a Monte Carlo treatment planning system. However, the reconstruction method is an inverse radiation transport problem which is poorly conditioned, in the sense it may become unstable due to small perturbations in the input data. Predicting the sharp (delta-like) peak in the electron spectrum provides an additional challenge for the numerical reconstruction technique. To improve efficiency and robustness of the reconstruction technique, we developed an algorithm based on a separation of the electron spectrum into singular and regular components. We approximate the singular peak of the spectrum by a narrow weighted Gaussian function. The parameters of this Gaussian function are sought using only the fall-off and toe regions of the depth-dose curve. Analytical representation of the spectral peak by a Gaussian has benefit since only one weight and the mean and variance must be derived from the depth-dose curve instead of multiple spectra weights. The regular part of the spectrum is reconstructed from the residual depth-dose distribution using a variational method combined with a regularization technique to avoid the nonphysical oscillations. The effectiveness of the method is demonstrated by comparing predictions to ''benchmark'' spectra and depth-dose distributions from Monte Carlo simulation of medical accelerators.
[DOI: 10.1118/1.1461840]

Key words: electron, depth dose curve, transport equation, inverse problem

I. INTRODUCTION

Energy spectra of medical accelerators significantly affect the pattern of dose distributions in patients undergoing radiotherapy treatment. Currently, electron spectra are taken into account implicitly using the measured central axis depth-dose curve which is included into pencil beam algorithms. In the near future, more advanced Monte Carlo treatment planning systems may appear in clinics which will simulate the 3D electron–photon transport more accurately using CT-defined patient geometry. Simulation of 3D electron transport using CT numbers requires the energy spectra and angular distribution of electrons from medical accelerators on the patient surface in explicit form.

Energy spectra and angular distribution of electrons from medical accelerators may be measured directly or obtained from the Monte Carlo simulation of the accelerator treatment head.[1,2] However, these two direct ways of obtaining the energy-angular distributions are not commonly implemented into routine clinical praxis primarily because of the complexity of measurement and the knowledge base required for running Monte Carlo simulations. Therefore, many investigators have tried inverse reconstruction to derive electron beam parameters from the measured data such as the central axis depth dose curves which are already included into the standard commissioning procedure for medical accelerators.[3–8] There are several advantages to using inverse reconstruction. First, it does not require any supplementary equipment or detailed knowledge of the treatment head composition and geometry. Second, the equipment for measurement of the dose distributions is standard and already available in any clinic. Third, these methods are computationally fast.

Although a very attractive tool for clinical commissioning of a Monte Carlo treatment planning system, reconstruction of the phase-space distribution of an incident electron beam from depth-dose curves and lateral dose profiles is a difficult numerical problem. The identification of the parameters of a radiation source with a limited number of external detectors is akin to *inverse radiation transport problems* which are notorious for being poorly conditioned, in the sense they may become unstable to small changes in the input data. Moreover, the computational finite arithmetic may impose additional practical limitations to the calculation algorithm. Also, the specific from of electron spectra provides an additional challenge for the numerical reconstruction technique because of the problems with sharp (delta-like) energy peaks of direct electrons. Finally, inverse reconstruction of electron beam parameters from depth-dose curves and lateral profiles is a multidimensional problem because their shape depends on both the energy and angular distributions of the incident electrons.

In this study, we consider only one part of this inverse problem, namely the reconstruction of an energy spectrum

from the central axis depth dose curve. We also suppose that the energy deposition from the treatment head bremsstrahlung is already subtracted from the total energy deposition. Under these conditions, the problem reduces to the integral Fredholm equation of the first kind for the incident electron spectrum and, in this sense, is similar to the previously considered reconstruction of photon spectra.[9,10] However, the electron spectrum is distinguished by a high-intensity singular component due to direct electrons and a low-intensity regular component due to electrons scattered with large energy loss. The difference between intensities in the singular and regular components is several orders of magnitude. Therefore, the form of electron spectra and also the physics of electron transport require special approaches in the reconstruction technique.

It is a common procedure in the reconstruction of electron spectra to introduce an energy grid and characterize the spectrum by its integrals over the energy bins. In this article, we refer to this method as a spectral weight technique. The spectral weight technique with different methods for solving the integral Fredholm equation of the first kind was used by Zhengming and Jette,[3] Faddegon and Blevis,[4] and Deng *et al.*[5] The spectral weight technique is universal because it is suitable for simulation of any complicated form of energy spectra. However, it inevitably will have problems with the steep gradients and sharp peaks in an energy spectrum. Also, the spectral weight technique may become unstable because of the ill-conditioning property of the integral Fredholm equation of the first kind which governs the reconstruction procedure. The importance of the regularization techniques to correct for the ill-conditioning property was pointed out by Zhengming and Jette.[3]

An alternative approach to the reconstruction of electron spectra was used by Kawrakow *et al.*[7] In this approach, parameters of the analytic trial functions are sought instead of the multiple spectral weights. The form of the trial functions can be easily selected because the general form of electron spectra of medical accelerators is well known. The analytic technique is stable if, of course, the number of trial functions and their parameters are relatively small. The analytic technique is more effective for the spectral peak and less effective for the low-energy part of the spectrum because the low-energy part has a complicated form defined by the electron scattering from the treatment head and applicator. The low-energy part of electron spectrum cannot be described by a simple analytic function with a few parameters.

The main goal of this article is to improve the accuracy and robustness of electron energy spectra reconstructed from measured depth dose distributions. To achieve this goal, we develop a hybrid method which has the advantages inherent to both the spectral weight and analytical techniques.[8] The main idea of the method is based on the fact that a large component of the electron spectrum can be described by a simple analytical function and separated from the numerical reconstruction. These electrons are mostly direct electrons which did not undergo scattering with large energy loss. The delta-like distribution of direct electrons presents a major problem for the numerical reconstruction techniques. We approximate this delta-like distribution by a weighted Gaussian. The residual component of the spectrum that is smooth and regular is reconstructed numerically using the spectral weight approximation. The integral Fredholm equation of the first kind is solved using a variational method combined with different regularization techniques to correct for the ill-conditioned property.

The developed technique is applied to ''benchmark'' problems with known depth dose distributions and energy spectra for a Philips-Elekta SL75-20 and a Varian Clinac 2100C medical accelerators. The energy spectra and depth-dose distributions for these accelerators have been obtained by Ding and Rogers using EGS4/BEAM Monte Carlo treatment head simulation.[11] The Monte Carlo ''benchmark'' data have been selected for the validation of our reconstruction technique because the electron energy distribution is available over all the energy range. Also, the depth-dose curve due to the treatment head bremsstrahlung is explicitly available in these calculations.

The remainder of this article is organized as follows. In Sec. II, we describe the depth-dose models for reconstruction of electron spectra, a variational method with regularization for solving the inverse problem for the depth-dose curve and the preparation of monoenergetic response functions using the discrete ordinates method. In Sec. III, we present an analytic singular component decomposition technique to improve the accuracy of reconstructed spectra. In Sec. IV, we discuss the reconstructed spectra for different medical accelerators. Finally, we give conclusions in Sec. V.

II. SOLVING THE INVERSE PROBLEM FOR THE ELECTRON DEPTH-DOSE CURVE

A. Equations for the electron depth-dose curve

Reconstruction of an electron spectrum from a measured central axis depth-dose distribution of a broad beam is based on numerical solutions to the integral Fredholm equation of the first kind,

$$D(z)=\int_0^{E_{\max}} f(E)d(z,E)\,dE, \tag{1}$$

where $D(z)$ is the measured central-axis depth-dose distribution in a water phantom, $f(E)$ is the electron spectrum of incident electrons, and $d(z,E)$ is the depth dose distribution from the monoenergetic beam with energy E. In practical measurements, the depth-dose distribution $D(z)$ contains a component of the order of a few percent that is due to the treatment head bremsstralung. Effective algorithms for the decomposition of energy deposition due to treatment head bremsstrahlung already have been considered by Faddegon and Blevis[4] and Deng *et al.*[5] In this article, we suppose that the depth-dose distribution due to treatment head bremsstrahlung is already subtracted from the total depth-dose distribution.

For the numerical approximation of Eq. (1), we introduce an energy grid $[E_{n-1/2},E_{n+1/2}]$, $n=1,...,N$, where $E_{1/2}=0$, $E_{N+1/2}=E_{\max}$ and $E_n=0.5(E_{n-1/2}+E_{n+1/2})$, $n=1,...,N$. We

suppose that the energy intervals are narrow enough that within each interval the following condition holds: $d(z,E) \approx d(z,E_n)$ where $d(z,E_n)$ is the depth dose distribution from a monoenergetic source with energy E_n. Then integrating Eq. (1) over the energy grid we obtain a numerical approximation

$$D(z)=\sum_{n=1}^{N} w_n d(z,E_n), \tag{2}$$

where the spectral weights w_n, $n=1,...,N$, are given by

$$w_n=\int_{E_{n-1/2}}^{E_{n+1/2}} f(E)dE, \quad n=1,...,N. \tag{3}$$

In the approximation given by Eqs. (2) and (3), reconstruction of the incident electron spectrum reduces to that of finding a discrete number of spectral weights w_n, $n=1,...,N$.

The model for calculation of monoenergetic depth dose distributions $d(z,E_n)$ significantly affects the accuracy of the reconstructed spectra. For instance, electrons incident on the patient surface are characterized not only by the energy spectrum but also by significant angular spread. It is usually supposed that the form of the depth-dose distribution is mostly due to the energy spectrum and is not affected by the angular spread.[3–5] In this approximation, the monoenergetic depth-dose function $d(z,E_n)$ can be calculated in the *RZ* geometry with the point source on the axis *Z* or in the parallel broad beam geometry using an inverse square factor. Both models correspond to a monodirectional source at the phantom surface. Definitely, the *RZ* geometry is more accurate but the parallel broad beam geometry is less expensive. Because the parallel broad beam geometry is less expensive a higher precision for the depth-dose distributions can be achieved for the same computational time.

To verify accuracy for the parallel broad beam model and to investigate the influence of the initial angular spread on the depth-dose distributions, we have compared depth-dose curves from complete EGS4/BEAM simulations and simulations in the parallel broad beam geometry using input EGS4/BEAM incident spectra. The coupled electron–photon transport in the parallel broad beam geometry with EGS4/BEAM spectra was simulated using the standard discrete ordinates package CEPXS/ONELD-1.0 that is discussed later in this article. An example of such a comparison for 6, 9, and 18 MeV beams from a Varian Clinac 2100C accelerator is presented in Fig. 1. The depth-dose distribution of treatment head bremsstrahlung was subtracted from the central axis depth-dose curves simulated using the EGS4/BEAM code. Also, these central axis depth-dose curves have been corrected for the inverse squared factor.

The agreement between EGS4/BEAM and CEPXS/ONELD-1.0 simulations is almost perfect for the 9 and 18 MeV beams in the fall-off and toe regions of the depth-dose curve. This is the region where the difference is expected to be significant due to the different treatment for the divergence of the electron beam. Thus, we can conclude from this comparison that the parallel broad beam geometry is acceptable in the simulation of the monoenergetic depth-dose functions $d(z,E_n)$.

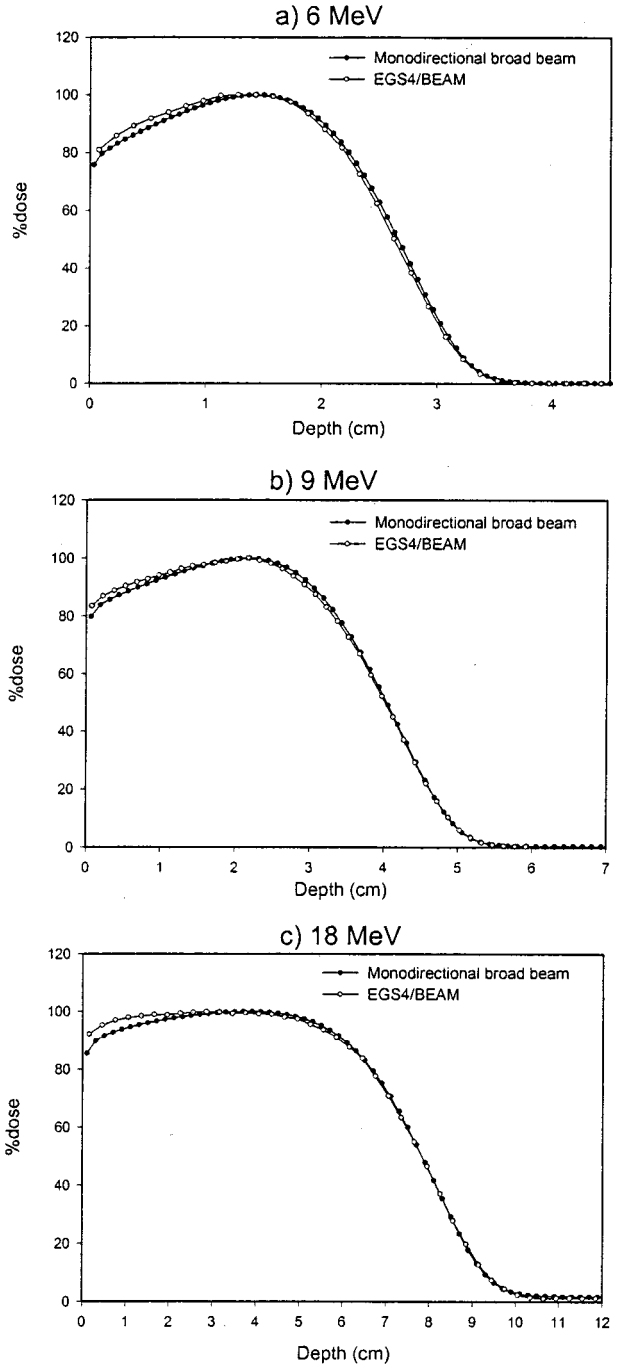

FIG. 1. Comparison of the central axis depth-dose curves calculated using the EGS4/BEAM code for 6 (a), 9 (b), and 18 (c) MeV electron beams from a Varian Clinac 2100C accelerator[11] and the depth-dose distributions of monodirectional broad beams with identical incident energy spectra. The central depth-dose curves from the EGS4/BEAM simulation are corrected for the treatment head bremsstrahlung and the divergence of electron beam. The monodirectional broad beam simulation is performed using the discrete ordinates package CEPXS/ONELD-1.0 with the incident electron spectrum taken from EGS4/BEAM treatment head simulation.

The curves simulated in the parallel broad beam geometry follow closely those simulated with the EGS4/BEAM code,

so the form of the depth-dose curves is primarily due to the form of the incident energy spectra. However, there is discrepancy of the order of few percent in the plateau region which increases as the surface is approached. This discrepancy cannot be explained by the divergence of the beam since the inverse square factor approaches zero at the surface. Therefore, we conclude that the large angular spread of electrons scattered with large energy loss has a noticeable influence on the shape of the depth-dose distributions. For the 6 MeV beam, there is also a discrepancy in the fall-off region because at this low beam energy the angular spread is significant even for the direct electrons.

If the monodirectional depth-dose curves are used for the reconstruction of energy spectrum from the measured or EGS4/BEAM central axis depth dose curve, this will result in an ''effective'' energy spectrum. In the ''effective'' energy spectrum, the effect of initial angular spread is simulated by ''softening'' of the spectrum, so the ''effective'' energy spectrum will produce a desirable depth-dose distribution. However, it is not clear how this artificial ''softening'' of the spectrum will affect the lateral profile and the accuracy in 3D calculations. If 1% dose/1 mm position accuracy is a goal for the electron dose calculations, the initial angular spread must be taken into account in the spectrum reconstruction procedure.

Instead of the energy spectrum alone, the incident electron beam should be characterized by the angular-energy-dependent electron source $Q(E,\mu)$ where $\mu=\cos\theta$ and θ is the angle between the normal to the water surface and direction of the incident electron. The energy and angular dependence of this source simulates the scattering of electron beam in air and from the components of the treatment head and applicator. If the angular distribution of the electron source is assumed to be asymuthally symmetric, then the depth dose distribution from this source may be expressed as follows,

$$D(z)=\int_0^{E_{\max}}\int_{-1}^{+1} Q(\mu,E)\overline{d}(z,\mu,E)\,d\mu\,dE, \tag{4}$$

where the energy-angular depth-dose function $\overline{d}(z,\mu,E)$ represents the dose distributions from the monoenergetic elementary sources with energy E_0 and angle of incidence μ_0,

$$q(\mu,E)=\delta(E-E_0)\,\delta(\mu-\mu_0). \tag{5}$$

Obviously, the complete reconstruction of the initial energy–angular distribution $Q(E,\mu)$ using only a depth-dose curve $D(z)$ is not possible. The angular distribution must be determined from an analysis of the lateral dose profiles or a simplified consideration of the treatment head. Then, it should be taken into account in the reconstruction of electron spectra. If the energy–angular distribution of incident electrons in each energy interval $[E_{n-1/2},E_{n+1/2}]$ is expressed in the form

$$Q_n(\mu,E)=f_n(E)\chi_n(\mu),\quad n=1,...,N, \tag{6}$$

where $f_n(E)$ is the energy spectrum and $\chi_n(\mu)$ is the angular distribution, we obtain for the depth dose distribution an equation similar to Eq. (4) with the elementary depth-dose distributions given by

$$d(z,E_n)=\int_{-1}^{1}\overline{d}(z,\mu,E_n)\chi_n(\mu)\,d\mu. \tag{7}$$

The weighting of the depth-dose distributions with the angular distributions $\chi_n(\mu)$, $n=1,...,N$, is important for the reconstruction of the low-energy part of the spectrum where electrons have considerable angular spread due to scattering from the applicator. It is less important for the reconstruction of the high-energy part of the spectrum where electrons have a small angular spread due to scattering in air.

The reconstruction of an energy spectrum given by the weights w_n, $n=1,...,N$, and the angular distributions $\chi_n(\mu)$, $n=1,...,N$, may be considered as two separate problems. First, we determine the angular distributions $\chi_n(\mu)$, $n=1,...,N$, and find the weighted depth dose distribution. Then, second, solve Eq. (2) for the spectral weights. The main goal of this article is to find an accurate and robust algorithm for solving Eq. (2). So, we will suppose that the incident electrons do not have the angular spread, i.e., the angular distribution is $\chi_n(\mu)=\delta(\mu-1)$, $n=1,...,N$. Also, to verify our algorithm, we use the depth-dose curves which are calculated with the EGS4/BEAM spectra and for monodirectional electron beams.

B. A variational method with regularization

Solving the integral Fredholm equation of the first kind for the electron spectrum $f(E)$ is possible using several numerical techniques. In application of these techniques, it should be recognized that the integral Fredholm equation of the first kind is ill conditioned on the depth-dose distribution $D(z)$. This ill-conditioned property may produce large nonphysical oscillations in the reconstructed spectrum $f(E)$ due to small errors in the depth-dose distribution $D(z)$ and truncation errors of the numerical techniques. The amplitude of oscillations may vary from one method to another and even can be reduced by use of adaptive energy grids, as was done by Faddegon and Blevis.[4] However, the results will be unstable and unpredictable if the source of these oscillations, which is in the equation itself, is not removed.

The ill-conditioned property of the integral Fredholm equation of the first kind can be demonstrated by implementation of a high-frequency perturbation with a limited amplitude $\delta f(E)=\exp(i\omega E)$, $\omega>0$, into the spectrum $f(E)$. Substituting this perturbation into Eq. (1) and integrating by parts we obtain for the corresponding perturbation in the depth dose distribution

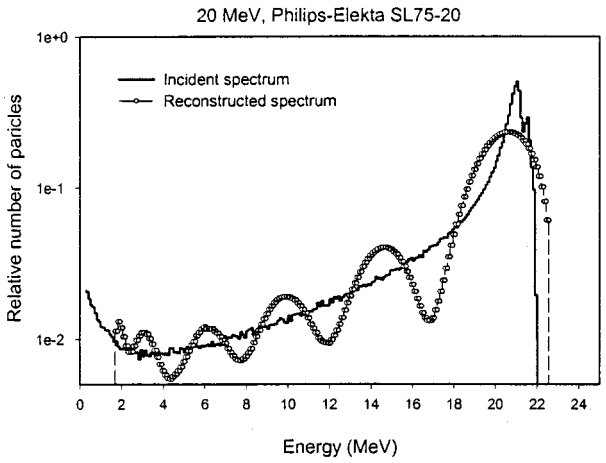

FIG. 2. Comparison between the incident electron spectrum and the spectrum reconstructed from the depth-dose distribution in water using the spectral weight technique without regularization. The incident electron spectrum is for to the 20 MeV electron beam from an Philips-Elekta- SL75-20 accelerator.[11]

$$\delta D(z)=\int_0^{E_{\max}} d(z,E)e^{i\omega E}\,dE$$

$$=\frac{1}{i\omega}e^{i\omega E}d(z,E)\Big|_0^{E_{\max}}-\frac{1}{i\omega}\int_0^{E_{\max}}\frac{\partial d(z,E)}{\partial E}e^{i\omega E}\,dE$$

$$=O\left(\frac{1}{\omega}\right). \tag{8}$$

The perturbation $\delta D(z)=O(1/\omega)$ can be very small for the high frequencies $\omega>0$. It follows from this analysis that very small perturbations in the depth-dose distribution can produce large high-frequency perturbations in the spectrum. If the errors of the depth dose distributions are negligible, but the problem is solved numerically, truncation errors are inevitable. Again, it can lead to large errors in the spectrum. Figure 2 shows large periodic oscillations in the reconstructed electron spectrum generated by small errors in the depth-dose distribution and, probably, by numerical approximations. The incident electron spectrum used for this figure corresponds to the 20 MeV electron beam from a Philips-Elekta SL75-20 accelerator.[11]

To correct for the ill-conditioned property of the integral Fredholm equation of the first kind, special regularization techniques have been developed. The main idea of these methods is to find a stable operator with a solution that approximates the solution to the integral Fredholm equation of the first kind. In this article, we apply a variational method for solving Eq. (2) where a least squares objective function is minimized using simple constraints on the spectrum. A spatial Tichonov's regularization function is included into the objective function to achieve stability of the reconstructed spectrum.[12] The final equation for the objective function is given by

$$\Theta_m[f(E)]=\int_0^{z_{\max}}(\overline{D}(z)-D(z))^2\,dz+\alpha\Omega_m[f(E)], \tag{9}$$

where $\overline{D}(z)$ is the measured depth dose distribution, $\Omega_m[f(E)]$ is the regularization function, and α is the regularization parameter. The non-negative source $f(E)$ that will minimize the objective function $\Theta_m[f(E)]$ will give a solution to the inverse problem of the depth-dose curve. We write this problem as

$$\min\Theta_m[f(E)], \quad \text{subject to} \quad f(E)\geqslant 0. \tag{10}$$

The regularization function $\Omega_m[f(E)]$ in Eq. (9) is given by

$$\Omega_m[f(E)]=\int_0^{E_{\max}}dE\sum_{k=0}^{m}p_k(E)\left(\frac{d^k f(E)}{dE^k}\right)^2, \tag{11}$$

where $p_k(E)$ is a positive continuous weighting function which is usually $p_k(E)\equiv 1$. The stabilizing function with $m=0$ corresponds to the *weak* regularization that provides only mean squared convergence $f^{\alpha}(E)\rightarrow f(E)$. The stabilizing function with $m\geqslant 1$ corresponds to the *strong* regularization that provides uniform convergence of the energy spectrum $f^{\alpha}(E)\rightarrow f(E)$ together with its derivatives of the maximum order $(m-1)$. In practical calculations, they use values not higher than $m=1$ because the values $m>1$ lead to excessive smoothing of the reconstructed function. The regularization parameter α in Eq. (9) is commonly selected by visual control. The smallest value of α is selected which mitigates the nonphysical oscillations in the reconstructed spectrum.

The minimum of the objective function given by Eq. (9) is found using the L-BFGS-B code which has been developed at the Optimization Technology Center, a joint venture of Argonne National Laboratory and Northwestern University. The code is based on the L-BFGS-B algorithm which is a limited-memory version of the quasi-Newton method with simple constraints on the variables.[13] The method is very convenient for practical use because it requires only an objective function and its derivatives as input to perform the minimization search. The gradients for the objective function given by Eqs. (9) and (11) are presented in Appendix A.

Examples of the iterative numerical reconstruction of electron spectra are shown in Figs. 3(a) and 3(b). The iterative processes have identical initial particle distribution. We see that the reconstruction without regularization [Fig. 3(a)] is unstable and the reconstruction with regularization [Fig. 3(b)] is stable. The benchmarch problem is for the 20 MeV electron beam from a Philips-Elekta SL75-20 accelerator.

C. Generation of the response function $d(z,E)$ using the discrete ordinates method

One of the key elements in the numerical solution of Eq. (1) is an adequate approximation of the response function $d(z,E)$ by a set of monoenergetic depth-dose curves $d(z,E_n)$, $n=1,...,N$. First, the energy intervals $[E_{n-1/2},E_{n+1/2}]$, $n=1,...,N$, must be narrow enough to accurately approximate the reconstructed spectrum and the equation $d(z,E)\approx d(z,E_n)$ must be valid within each energy interval. Second, the precision of the depth-dose curves

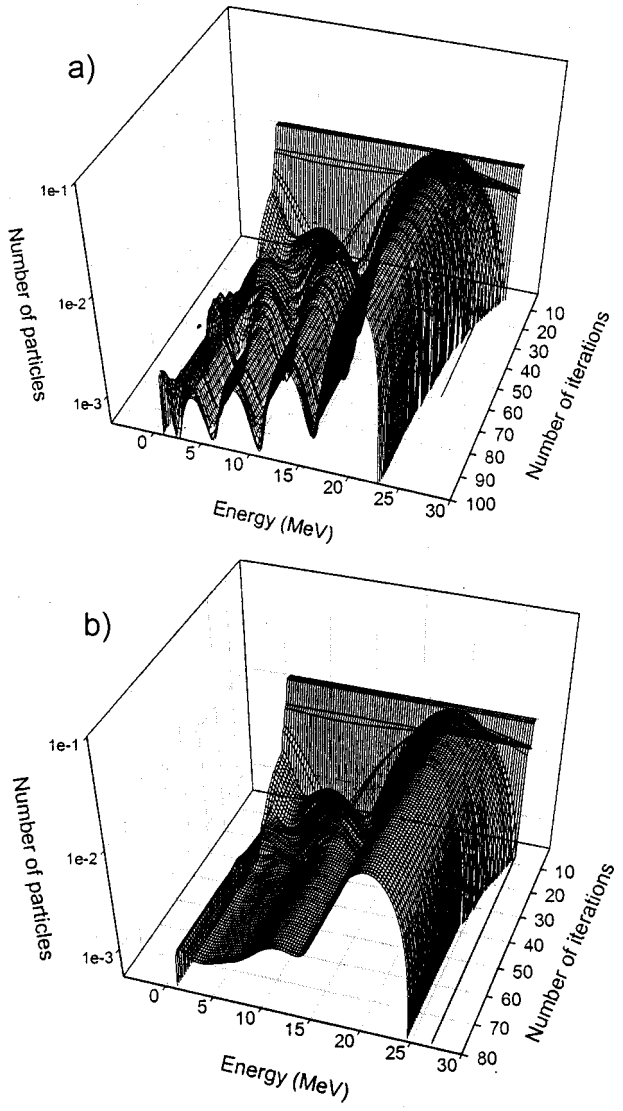

FIG. 3. Examples of the iterative numerical reconstruction of the electrun spectrum without regularization (a) and using regularization (b).

$d(z,E_n)$, $n=1,...,N$, must provide accurate calculation of the gradients for the objective function and uniform convergence of the iterative search process. Our experience shows that a uniform discretization with energy steps of 0.125 MeV from 0 to 25 MeV (i.e., 200 monoenergetic depth-dose curves) is adequate for accurate reconstruction of the electron spectra from medical linear accelerators. Further refinement of the energy grid does not improve the reconstructed energy spectra.

However, if the angular distribution $\chi_n(\mu)$, $n=1,...,N$, of incident electrons must be taken into account, the angular-energy-dependent response function $\overline{d}(z,\mu,E)$ must be calculated. The angular-energy-dependent response function $\overline{d}(z,\mu,E)$ must be folded with angular distributions $\chi_n(\mu)$, $n=1,...,N$ [see Eq. (7)], to produce depth-dose distributions of improved accuracy. In this case, calculation overhead will significantly increase. For instance, using 20 angular points from 0° to 90° to approximate the large-angle scattering of electrons, the total number of depth-dose curves in the algorithm should be $20\times200=4000$. Therefore, the calculation of the dose functions $d(z,E)$ and $\overline{d}(z,\mu,E)$ is a specific transport problem where a great number of depth-dose distributions must be calculated in a very simple geometry and with very high precision.

The monoenergetic depth-dose curves can be calculated using the condensed-history Monte Carlo method which is considered a standard numerical technique for the coupled electron-photon transport. Deterministic (i.e., nonstochastic) methods for the coupled electron-photon transport are also available.[14] Despite the promising theoretical consideration of Borgers,[15] deterministic methods are still less effective in complicated geometries than Monte Carlo methods. However, they may be more efficient than the Monte Carlo method for some specific problems in simple geometries. For instance, the response function $d(z,E)$ can be simulated very fast with high accuracy using the discrete ordinates method.

The discrete ordinates method is a deterministic method for explicitly solving the Boltzmann transport equation. Standard discrete ordinates codes find numerical solutions to the transport equation using an S_n approximation in angle (n angular segments), a multigroup approximation in energy, and some form of spatial differencing. The discrete ordinates solution converges to the analytical solution as more groups, spatial meshes, and discrete angles are employed. One of the advantages of the discrete ordinates method is the accuracy with which the particle distributions are generated. This accuracy is usually defined by the convergence parameter for the iterations on the scattering source and is of the order of 0.01% in all calculational regions. In the Monte Carlo calculations, a precision of 1% at the maximum of the electron depth-dose curve is considered acceptable. The precision can be worse in the fall-off and the toe regions of the depth-dose curve which are characterized by deep penetration of particles. Another advantage of the discrete ordinates method is the speed of calculations. In the predictions of the depth-dose distributions, the discrete ordinates method can be 50 times faster than the Monte Carlo method.[16–18] The extremely high accuracy and calculational speed of the discrete ordinates method motivated us to use this method for the generation of the response function $d(z,E)$.

The coupled electron–photon transport calculations in this article were performed using the package CEPXS/ONELD-1.0 which is based on the multigroup discrete ordinates method.[16–18] The package CEPXS/ONELD-1.0 was developed for simulation of the coupled electron–photon transport in one-dimensional geometries. It consists of the code CEPXS for the preparation of the coupled multigroup electron–photon crosssections and the general purpose one-dimensional Boltzmann transport solver ONEDANT which was previously developed for solving the neutron–photon transport problems. The CEPXS/ONELD-1.0 discrete ordinates package solves the time-independent coupled electron–photon–positron problems in plane, spherical, and cylindrical geometries. For the neutral particle (photon) transport the Boltzmann equation is solved

$$\mathbf{\Omega}\cdot\nabla\Psi_\gamma+\Sigma_t^\gamma\Psi_\gamma=\int_0^\infty dE'\int_{4\pi}d\mathbf{\Omega}'\Sigma_{\gamma\gamma}(\mathbf{r},E'\rightarrow E,\mathbf{\Omega}'\cdot\mathbf{\Omega})\Psi_\gamma(\mathbf{r},E',\mathbf{\Omega}')+\int_0^\infty dE'\int_{4\pi}d\mathbf{\Omega}'\Sigma_{e\gamma}(\mathbf{r},E'\rightarrow E,\mathbf{\Omega}'\cdot\mathbf{\Omega})\Psi_e(\mathbf{r},E',\mathbf{\Omega}'),\tag{12}$$

and for the charged particle (electron and positron) transport the Boltzmann-CSD (continuous slowing down) equation is solved

$$\mathbf{\Omega}\cdot\nabla\Psi_e+\Sigma_t^e\Psi_e=-\frac{\partial}{\partial E}[S_e(\mathbf{r},E)\Psi_e]+\int_0^\infty dE'\int_{4\pi}d\mathbf{\Omega}'\Sigma_{ee}(\mathbf{r},E'\rightarrow E,\mathbf{\Omega}'\cdot\mathbf{\Omega})\Psi_e(\mathbf{r},E',\mathbf{\Omega}')+\int_0^\infty dE'\int_{4\pi}d\mathbf{\Omega}'\Sigma_{\gamma e}(\mathbf{r},E'\rightarrow E,\mathbf{\Omega}'\cdot\mathbf{\Omega})\Psi_\gamma(\mathbf{r},E',\mathbf{\Omega}').\tag{13}$$

In Eqs. (12) and (13), $\Psi_e\equiv\Psi_e(\mathbf{r},\mathbf{\Omega},E)$ and $\Psi_\gamma\equiv\Psi_\gamma(\mathbf{r},\mathbf{\Omega},E)$ are the spatial-angular-energy distributions of electrons and photons, $\Sigma_t^e\equiv\Sigma_t^e(\mathbf{r},E)$ and $\Sigma_t^\gamma\equiv\Sigma_t^\gamma(\mathbf{r},E)$ are the total cross sections for electrons and photons, $\Sigma_{ee}(\mathbf{r},E'\rightarrow E,\mathbf{\Omega}'\mathbf{\Omega})$ and $\Sigma_{\gamma\gamma}(\mathbf{r},E'\rightarrow E,\mathbf{\Omega}'\mathbf{\Omega})$ are the electron-to-electron and photon-to-photon differential in energy and angle cross sections, $\Sigma_{\gamma e}(\mathbf{r},E'\rightarrow E,\mathbf{\Omega}'\mathbf{\Omega})$ and $\Sigma_{\gamma e}(\mathbf{r},E'\rightarrow E,\mathbf{\Omega}'\mathbf{\Omega})$ are the electron-to-photon and photon-to-electron differential in energy and angle cross-sections, and $S_e(\mathbf{r},E)$ is the restricted stopping power which is the zeroth moment of the collisional and radiative cross sections with small energy transfers.

In the ONEDANT code, the Boltzmann transport equation (12) is solved by discretization of energy, space, and angular variables. The multigroup approximation for the energy dependence, S_n discrete ordinates approximation for the angular flux, and the Legendre P_L expansion for the angular dependence of cross sections are standard options in the discrete ordinates transport codes which have been used for many years in neutral particle transport. A revision of the ONEDANT code called ONEDANT-LD is recommended for solving the coupled electron–photon transport problems. This version is based on the third-order accuracy linear discontinuous (LD) spatial discretization. The LD spatial discretization provides numerical solutions of better quality, especially in the deep penetration problems, if compared to the standard second-order diamond difference (DD) spatial discretization. The final system of simple linear equations is solved iteratively with use of the S2 synthetic acceleration technique. The accuracy of solutions is defined primarily by the convergence of the iterative process and is of the order of 0.01%.

Having a better approximation order and improved monotonicity and positivity properties compared to the standard DD scheme, the LD scheme can become negative in computational cells with very steep gradients of solution. Usually, this problem is solved using nonlinear correction algorithms. The adaptive LD scheme is one of the ways to obtain a positive numerical solution without deterioration of source convergence inherent to other nonlinear algorithms.[19,20] Despite the fact that the nonlinear correction techniques for the LD scheme are theoretically available, the implementation of them into discrete ordinates codes is not easy because of problems with consistency in acceleration methods. None of the nonlinear corrections is available in the ONELD code. Therefore, the only way to avoid the negative solutions is to further refine the spatial grid.

The Boltzmann-CSD equation (13) was derived for solving the charged particle transport problems because the ''soft'' collisions with atomic electrons cannot be handled in the P_L and multigroup approximations. Also, differential cross sections are not adequate in this ''soft'' region, so only the moments of the cross sections can be estimated. A special technique was developed to solve the Boltzmann-CSD equation (13) using the standard discrete ordinates Boltzmann solvers as ONEDANT-LD.[21] The electron–photon cross sections in the multigroup and P_L Legendre approximations for solving the Boltzmann and the Boltzmann-CSD equations by the ONEDANT-LD code are generated by the CEPXS code using the same physical interactions which are usually taken into account in Monte Carlo calculations.

Lorence *et al.* demonstrated the accuracy and computational speed of the CEPXS/ONELD-1.0 package by comparison to the Monte Carlo predictions and experimental data.[18] The Monte Carlo predictions were obtained using one-dimensional codes of the Integrated-TIGER-Series (ITS). However, we find it useful to additionally compare CEPXS/ONELD-1.0 and Monte Carlo predictions in the problems which are specific to medical physics applications. These problems usually include water phantoms with bone-like heterogeneities and the energy of incident electron beams up to 20 MeV. Such a comparison for a water phantom and a water phantom with a slab SB3 bone-like heterogeneity is presented in Fig. 4. The normally incident broad electron beams are monodirectional and monoenergetic with energies 10 [Fig. 4(a)] and 20 [Fig. 4(b)] MeV. The benchmark problems and EGS4 calculations are from Neuenschwander *et al.*[22] The agreement between the Monte Carlo and discrete ordinates predictions is excellent, especially when it is taken into account that the numerical approaches for the nuclear crosssections and particle transport are quite different.

III. DECOMPOSITION OF THE SINGULAR COMPONENT

A. Complete decomposition

Electron energy spectrum from a medical accelerator may be separated into singular and regular components. The high-intensity singular component with delta-like energy distribution is due to direct electrons. The low-intensity regular component is due to electrons which are scattered with large

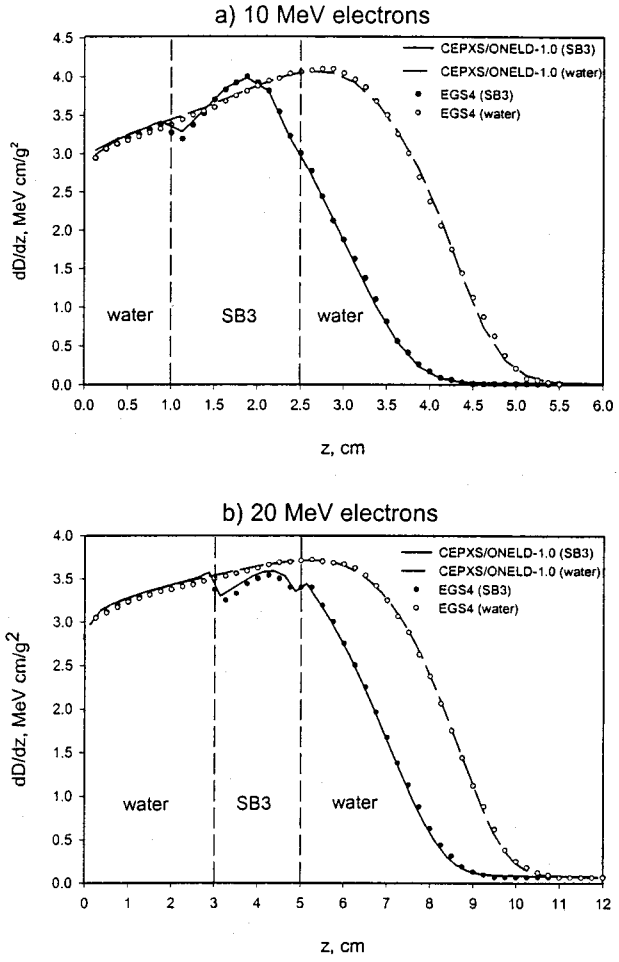

FIG. 4. Comparison between the depth-dose distributions in homogeneous and heterogeneous phantoms calculated using the EGS4 Monte Carlo code and the CEPXS/ONELD-1.0 discrete ordinates package for 10 MeV (a) and 20 MeV (b) monoenergetic and monodirectional broad electron beams. The EGS4 Monte Carlo simulations are taken from Neuenschwander *et al.*[22]

energy loss from the treatment head components and applicator. The singular component contains most of the electrons, so the difference of intensities in the regular and singular components is of several orders of magnitude. However, the regular component plays a significant role in the dose distributions because the integral number of electrons in this component is also significant.

Because of the specific form of the electron spectra the reconstruction technique based on the optimization of spectral weights with regularization is not always effective. There are several reasons for this: (1) The technique of spectral weights seems to be inefficient in describing the steep gradients associated with the spectrum's very sharp energy peak. Further refinement of the energy grid does not improve the accuracy because of the unavoidable errors in measured depth dose distributions and computed monoenergetic response functions. (2) It is well known that the regularization technique has a drawback of smoothing sharp peaks in a reconstructed function. Therefore, the spectral weight technique with regularization is not capable of reproducing the energy peak in the electron spectrum. (3) the spectral peak contains most of the electrons forcing the regular component to be affected by the numerical "noise" of the reconstruction technique. (4) The contribution of the fall-off region of the depth-dose curve to the least squares objective function is smaller than that of the plateau region. The contribution of the toe region of the depth-dose curve, critical for accurate reconstruction of the singular component, is much smaller. This means, that the gradient search is more accurate in the plateau region of the depth-dose curve for the objective function given by Eq. (9). Theoretically, the problem could be overcome by implementation of an importance weighting factor $I(z)=1/[\bar{D}(z)]^2$ into the objective function which would make all regions of the depth dose curve equally important in the objective function. We found, however, that this approach does not significantly improve the accuracy of reconstructed spectra.

It was concluded that the spectral weight technique might be very effective for the reconstruction of the regular component when the singular component is not present. This motivated us to use a hybrid reconstruction technique where the singular and regular components are processed using different approaches. We consider the electron energy spectrum as a sum of the singular $f^{\mathrm{reg}}(E)$ and the regular $f^{\mathrm{reg}}(E)$ components:

$$f(E)=f^{\mathrm{sing}}(E)+f^{\mathrm{reg}}(E). \tag{14}$$

Correspondingly, for the depth dose distribution $D(z)$ we have

$$D(z)=D^{\mathrm{sing}}(z)+D^{\mathrm{reg}}(z), \tag{15}$$

where $D^{\mathrm{sing}}(z)$ is the depth-dose from the singular component $f^{\mathrm{sing}}(E)$ of the spectrum and $D^{\mathrm{reg}}(z)$ is the depth-dose from the regular component $f^{\mathrm{reg}}(E)$ of the spectrum.

Instead of the spectral weight technique, the singular component of the spectrum is reconstructed using a single analytical function. In this article, we approximate the singular component of the spectrum by a narrow weighted Gaussian function,

$$f^{\mathrm{sing}}(E)=\lambda\,\frac{1}{\sqrt{2\pi}\sigma}\,e^{-(E-E_0)^2/2\sigma^2}, \tag{16}$$

where E_0 and σ are the mean energy and the variance and λ is a weighting factor. If the spectrum is normalized to one particle, the weight λ shows the relative number of particles in the singular component and the weight $(1-\lambda)$ shows the relative number of particles in the regular component. For the weighted Gaussian, only one weight and the mean and variance must be derived from the depth dose distribution instead of multiple spectral weights.

Parameters of the analytic approximation for the singular component are found using only the fall-off and toe regions of the depth-dose distribution. The parameters E_0, σ, and λ in Eq. (16) are found from the condition that the singular depth-dose component $D^{\mathrm{sing}}(z)$ approximates the fall-off and toe regions of the total depth dose $\bar{D}(z)$ as it is shown in Fig.

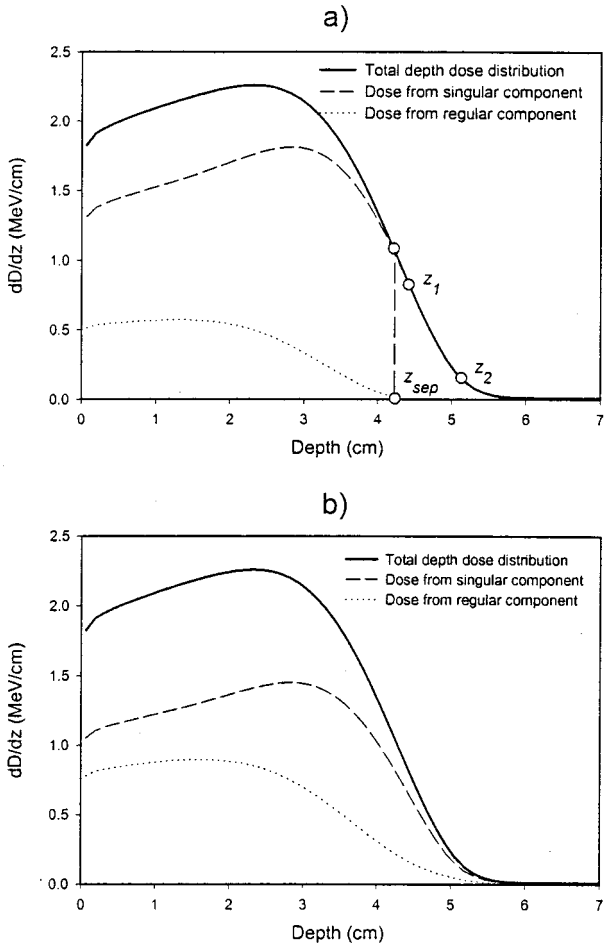

FIG. 5. Complete (a) and partial (b) decomposition of the singular dose component from the total depth-dose distribution. The total depth-dose distribution is for the 10 MeV electron beam from an Philips-Elekta- SL75-20 accelerator.[11]

5(a). The computational algorithm for solving this problem is based on the minimization of the following least squared objective function

$$\Phi[f^{\mathrm{sing}}(E)]=\int_{z_1}^{z_2}(\overline{D}(z)-D^{\mathrm{sing}}(z))^2\,dz, \tag{17}$$

where the coordinates z_1 and z_2 determine the region with dose deposition due to the singular component. The minimization problem

$$\min\Phi[f^{\mathrm{sing}}(E)], \quad \text{subject to} \quad f^{\mathrm{sing}}(E)\geqslant 0, \tag{18}$$

is solved using the same L-BFGS-B optimization routine which is used for the spectral weight technique. However, the optimization with an analytical Gaussian function does not require a regularization technique and is based on only three variables E_0, σ, and λ. The gradients for the L-BFGS-B algorithm which correspond to the objective function given by Eq. (17) and the analytical function $f^{\mathrm{sing}}(E)$ given by Eq. (16) are presented in Appendix B.

The regular part of the spectrum $f^{\mathrm{reg}}(E)$ is reconstructed using the spectral weight representation from the residual depth-dose distribution. The regular dose component $D^{\mathrm{reg}}(z)$ is found as a difference between the total depth-dose $D(z)$ and the singular depth-dose component $D^{\mathrm{sing}}(z)$. Applying the numerical reconstruction technique to the regular depth-dose component $D^{\mathrm{reg}}(z)$ we find the regular component of the spectra $f^{\mathrm{reg}}(E)$.

B. Partial decomposition

It should be noted that the complete separation of the singular component as it is shown in Fig. 5(a) is characterized by a separation depth z_{sep} which corresponds to the maximum range for electrons from the regular component. Because the separation depth z_{sep} is less than the maximum depth of penetration $z_{\max}$, there is also a separation energy $E_{\mathrm{sep}}<E_{\max}$ in the reconstructed spectrum that separates the regular and singular components. It is difficult to obtain a smooth junction between the regular and singular components in the point E_{sep} using complete separation of the singular component because any numerical algorithm will have problems with steep boundary conditions. Despite the nonphysical perturbations, the junction region does not have significant influence on the accuracy of the depth dose distributions. However, we try to avoid them using a partial separation of the singular component.

In the partial separation, a part of the singular component is transferred to the regular component and reconstructed numerically using the spectral weight technique. After determining the parameters λ, σ, and E_0 of the weighted Gaussian function given by Eq. (16) from the complete separation, we chose a new weighting parameter $\overline{\lambda}=\tau\lambda(0\leqslant\tau<1)$ and calculate new depth-dose distributions $D^{\mathrm{sing}}(z)$ and $D^{\mathrm{reg}}(z)$. Obviously, the value $\tau=0$ corresponds only to the numerical reconstruction technique that uses the spectral weights. The value $\tau=0.8$ was used in the calculations presented in this article. An example of partial separation is shown in Fig. 5(b). We see that the electrons from the regular and singular components penetrate till maximum depth $z_{\max}$, so there is no separation depth z_{sep}. Consequently, electrons in the regular and singular components have the same maximum energy $E_{\max}$ and we avoid the problem in the junction region. The energy spectra reconstructed from the depth–dose distributions in Fig. 5 are analyzed in Sec. IV.

IV. RESULTS

A. Computational parameters and grids

The reconstruction technique developed was applied to ''benchmark'' depth dose distributions which were calculated using the CEPXS/ONELD-1.0 code in parallel broad beam geometry. The incident electron spectra have been taken from EGS4/BEAM treatment head simulation for Philips-Elekta SL75-20 and Varian Clinac 2100C accelerators. As shown in Fig. 1, the difference between depth-dose distributions calculated using CEPXS/ONELD-1.0 in parallel broad beam geometry and complete EGS4/BEAM simulations is very small and is primarily due to the initial angular spread of the incident electrons. In this article, we do not consider the angular spread of incident electrons and use monodirec-

tional depth-dose functions $d(z,E_n)$. Therefore, to make the numerical experiment on the reconstruction of electron spectra absolutely ''pure'' we use depth-dose distributions calculated in the same geometry as the functions $d(z,E_n)$. Applying the reconstruction algorithm with the monodirectional functions $d(z,E_n)$ to the EGS4/BEAM depth-dose curves produces ''effective'' energy spectra which account for the initial angular spread of the incident electrons.

The monoenergetic response functions $d(z,E_n)$, $n=1,...,N$, have been calculated using the CEPXS/ONELD-1.0 discrete ordinates package over the energy interval 0.5–27 MeV with energy step 0.125 MeV, so the total number of depth-dose curves was $N=213$. Further refinement did not improve the accuracy of the reconstructed spectra. The accuracy of the calculated monoenergetic depth-dose curves was 0.01%, which corresponds to the convergence criterion of the discrete ordinates method. The depth-dose distributions were calculated in the space region from 0 to 15 cm for all energies, so the bremsstrahlung ''tail'' was accurately simulated up to a depth of 15 cm.

The coupled electron–photon transport was simulated using 50 equidistant energy groups for electrons and 30 equidistant energy groups for photons. The cutoff energy for electrons was 0.1 MeV. An S_{32} Gauss quadrature with 32 angular intervals was used for approximation of the angular flux and a P_{31} Legendre expansion was used for the angular dependence of the electron and photon cross-sections. The spatial dependence of the particle flux was calculated using 60 spatial meshes from the surface to the maximum range of electrons and 20–30 spatial meshes for the breamsstrahlung ''tail.'' The calculational time on a PENTIUM III 500 MHz computer was around 60 s for this discretization. Further refinement of the calculational grids did not improve the accuracy of depth-dose distributions.

The minimum of the objective functions based on the spectral weights and the weighted Gaussian function was found using the L-BFGS-B algorithm, which is a version of the deterministic quasi-Newton algorithm with simple constraints on the variables. For the objective functions and number of variables considered in this article, the typical calculational time is a few seconds on a PENTIUM III 500 MHz computer. To find an optimal solution, the algorithm uses as input the depth-dose curve and, additionally, the regularization parameter α for the objective function given by Eq. (9) and the depth coordinates z_1 and z_2 for the objective function given by Eq. (17). We found that the parameter $\alpha=0.125$ is suitable for regularization of any electron spectra if the energy bins $\Delta E=0.125$ MeV are used for approximation of the integral Fredholm equation of the first kind.

We also have to mention that weak regularization with the simplest weighting function $p(E)\equiv 1$ was effective enough, so we did not use the strong regularization. The depth coordinates z_1 and z_2 for the reconstruction of the singular component can be selected as $z_1\approx R_{40}$ and $z_2\approx R_{\max}$ where R_{40} is the depth where percent depth-dose drops off to 40% and $R_{\max}$ is the maximum range of the electrons.

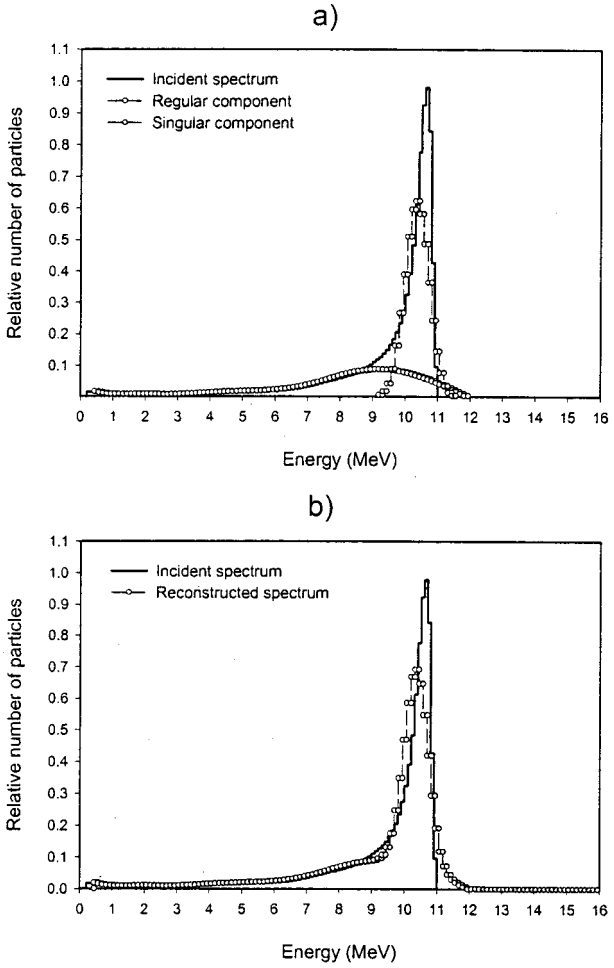

FIG. 6. The regular and singular components of the electron spectrum for the 10 MeV electron beam from a Philips-Elekta SL75-20 accelerator: (a) separated singular and regular components; (b) sum of the regular and singular components. The decomposition into regular and singular components corresponds to the decomposition of the depth-dose distribution presented in Fig. 5(b).

B. Analysis of the reconstructed spectra

Figure 6 shows the singular and regular components of electron spectrum [Fig. 6(a)] and the total electron spectrum [Fig. 6(b)] which have been reconstructed from the depth-dose distribution presented in Fig. 5. The incident electron spectrum corresponds to the 10 MeV electron beam of a Philips-Elekta SL75-20 accelerator. The y axis is linear in this plot to show the real ratio of the regular and singular components. The regular component of the reconstructed spectrum does not have noticeable nonphysical oscillations and approximates the low-energy part of the incident spectrum with good accuracy. The reconstructed singular component is slightly shifted to the low energies and the FWHM (full width at half maximum) is slightly overestimated. However, these discrepancies do not affect the accuracy of the depth-dose distributions calculated with the reconstructed spectrum because of the singular nature of this part of the spectrum. This accuracy is less than 1% over the electron range. It should also be understood that the reconstruction of

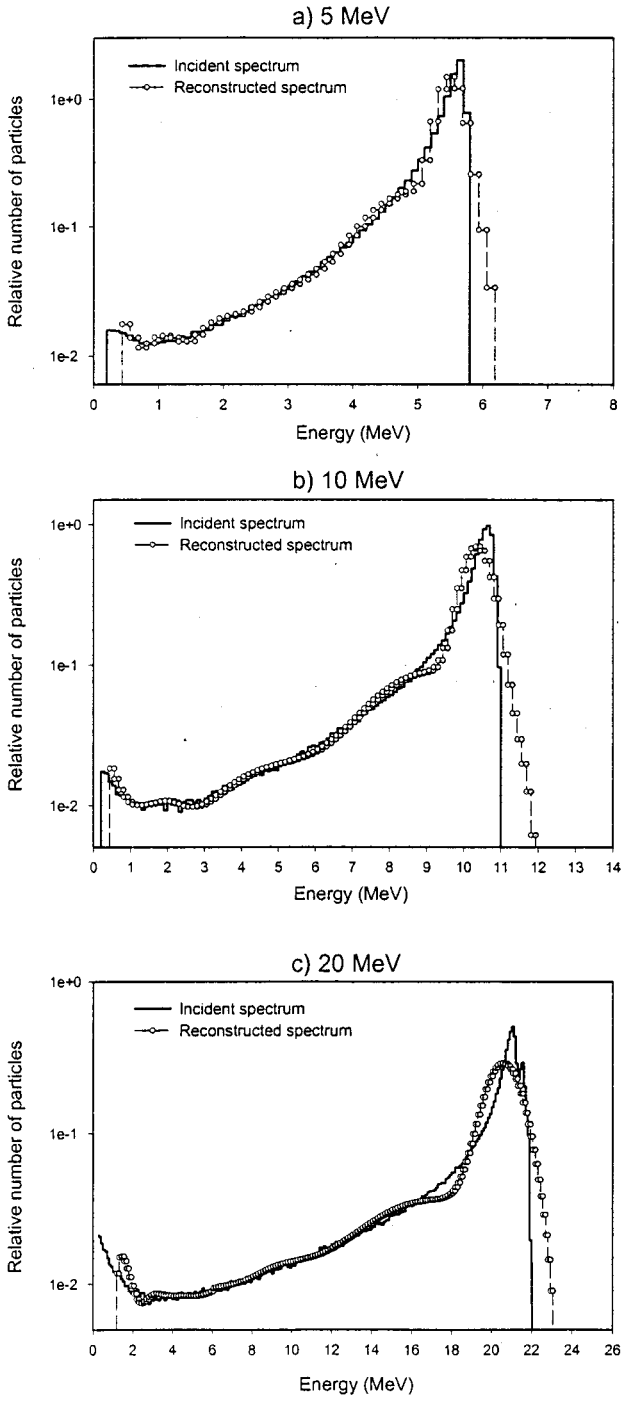

FIG. 7. Comparison of the incident and reconstructed electron spectra for the 5 (a), 10 (b), and 20 (c) MeV electron beams from a Philips-Elekta SL75-20 accelerator. The incident electron spectra were obtained by Ding and Rogers using Monte Carlo treatment head simulation.[11]

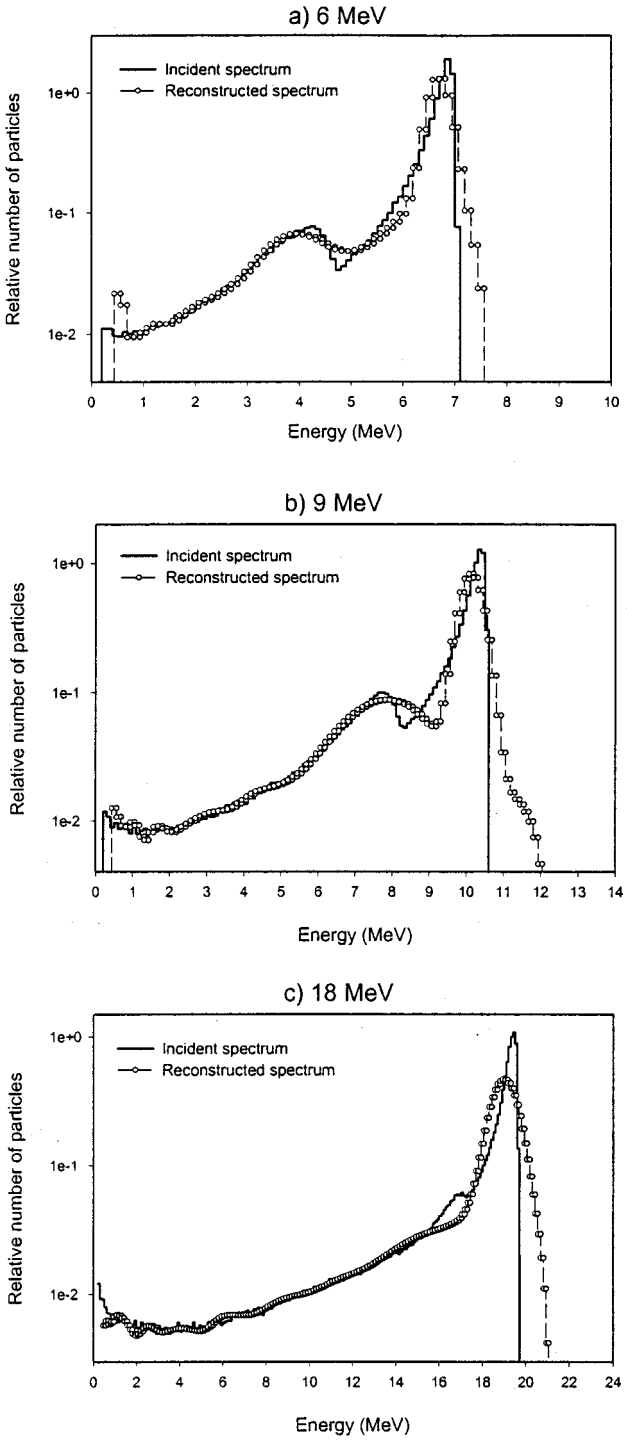

FIG. 8. Comparison of the incident and reconstructed electron spectra for the 6 (a), 9 (b), and 18 (c) MeV electron beams from a Varian Clinac 2100C accelerator. The incident electron spectra were obtained by Ding and Rogers using Monte Carlo treatment head simulation.[11] The *y* axis is logarithmic.

the singular component has a theoretical computational limit because of the small sensitivity of the depth-dose distribution to the form of the singular component.

Figure 7 show the incident and reconstructed electron spectra which correspond to the (a) 5, (b) 10, and (c) 20 MeV electron beams from a Philips-Elekta SL75-20 accelerator. The *y* axis is logarithmic in this plot to show the accuracy of the reconstructed regular component. The low-energy part is reconstructed with good accuracy for all energies. It seems that the algorithm reproduces even small statistical fluctuations in the incident Monte Carlo spectra. The accuracy in the peak region is lower and typically overestimates the FWHM. This overestimation decreases, however, with decreasing incident beam energy. The overestimation is primarily due to the computational limit of reconstruction of the

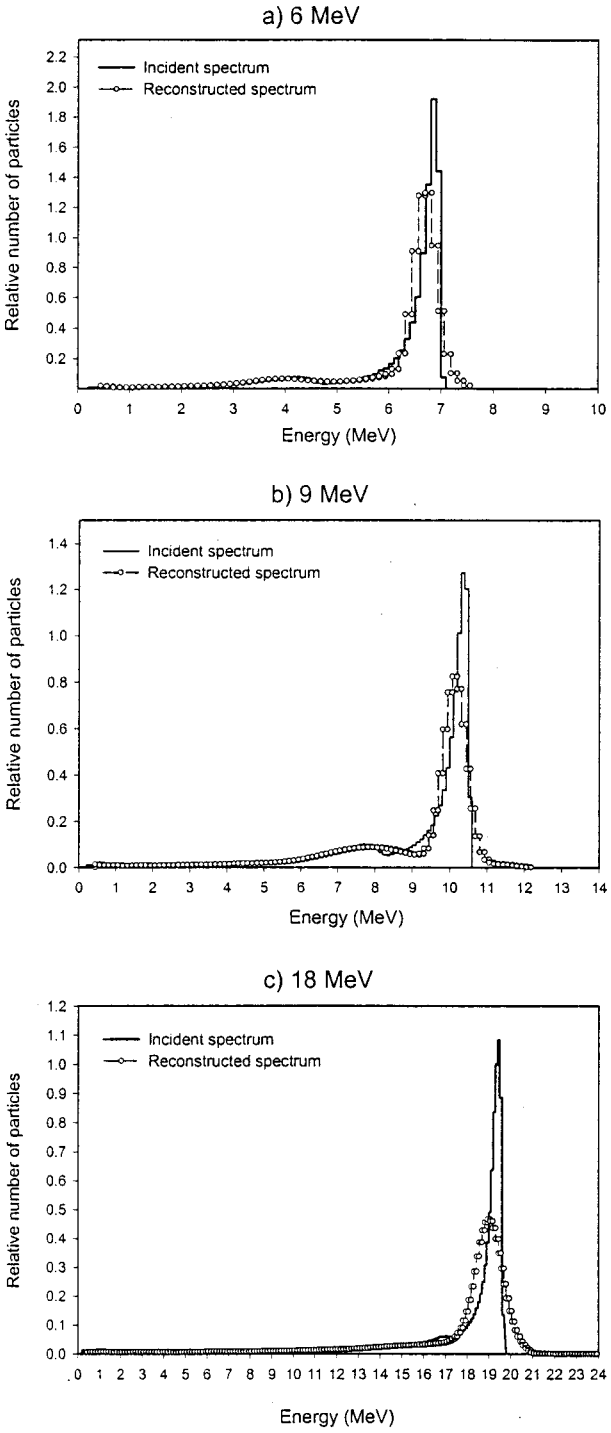

FIG. 9. Comparison of the incident and reconstructed electron spectra for the 6 (a), 9 (b), and 18 (c) MeV electron beams from a Varian Clinac 2100C accelerator. The incident electron spectra were obtained by Ding and Rogers using Monte Carlo treatment head simulation.[11] The *y* axis is linear.

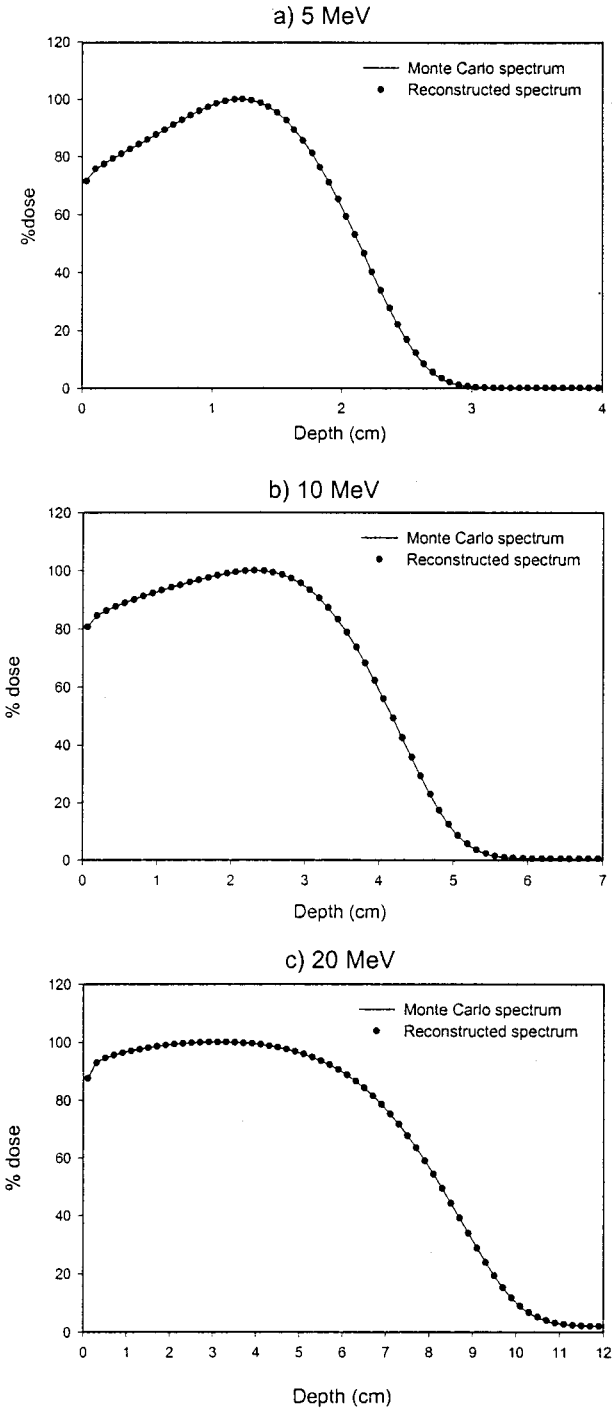

FIG. 10. Comparison of depth-dose curves calculated using Monte Carlo and reconstructed energy spectra for the 5 (a), 10 (b), and 20 (c) MeV electron beams from a Philips-Elekta SL75-20 accelerator. The spectra are shown in Fig. 7.

singular component. Our algorithm was able to reproduce the FWHM up to 5% of the mean energy which is smaller than theoretical limit of 10% previously reported by Feddegon and Blevis.[4] Probably, this improvement is due to the analytical approximation of the singular component and the accurate simulation of the depth-dose curve by the discrete ordinates method. Further improvement is hardly possible because of the small sensitivity of the depth-dose curve to variations in the value of the FWHM if the FWHM is less than 5%.

Figures 8 and 9 show the incident and reconstructed electron spectra which correspond to the (a) 6, (b) 9, and (c) 18 MeV electron beams from a Varian Clinac 2100C accelerator. We included additionally Fig. 9 with linear *y* axis to give clearly the relative size of the numerical artifacts. The results

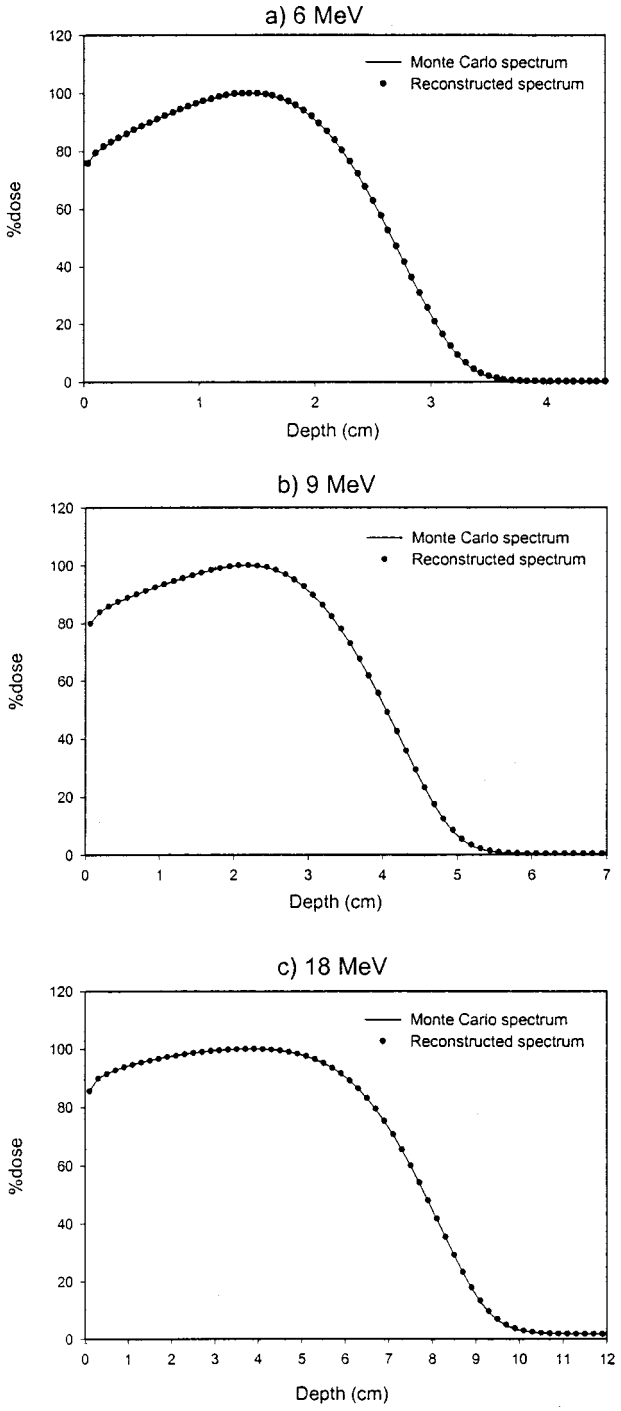

FIG. 11. Comparison of depth-dose curves calculated using Monte Carlo and reconstructed energy spectra for the 6 (a), 9 (b), and 18 (c) MeV electron beams from a Varian Clinac 2100C accelerator. The spectra are shown in Fig. 8.

are similar to those obtained for the Philips-Elekta SL75-20 accelerator with very good accuracy in the low-energy part of the spectra and overestimation of the FWHM of the peak. The resolution of the energy peaks improves with decreasing beam energy. Notice the reconstruction algorithm is capable of reproducing the second peak in the spectra for the 9 and 6 MeV beams which is due to electron scattering from the applicator. This second peak is, however, not reconstructed for the 20 MeV electron beam.

The depth-dose distributions calculated with the reconstructed spectra for both Philips-Elekta SL75-20 and Varian Clinac 2100C accelerators have a relative accuracy less than 1% over the electron range. A comparison of depth-dose distributions calculated using Monte Carlo and reconstructed energy spectra for these accelerators is presented in Figs. 10 and 11.

V. CONCLUSIONS

We have developed an algorithm for the reconstruction of electron spectra of medical accelerators from central axis depth-dose curves. Significant improvement of the robustness and accuracy of reconstructed spectra was achieved using separation of the singular and regular components of the electron spectrum. The algorithm is based on an effective variational method with regularization technique and a Gaussian analytical approximation for the singular peak of the electron spectrum. The regular component of the spectrum is reconstructed in close agreement with direct Monte Carlo simulations. Accuracy of the singular component is worse primarily due to the theoretical limit of reconstruction. This, however, does not affect the accuracy of the depth-dose distributions. The reconstructed electron spectra do not have nonphysical oscillations and reproduce the input depth-dose distributions with relative accuracy less that 1%. In order to be applied for commissioning of a Monte Carlo treatment planning system, the reconstruction algorithm must be supplemented by a method for determining the angular distribution of incident electrons.

ACKNOWLEDGMENTS

The authors would like to acknowledge Dr. G. X. Ding and Dr. D. W. O. Rogers for use of their data on the Monte Carlo simulation of five medical accelerators which they made available in digitized form on the Internet. We also acknowledge Dr. B. A. Faddegon of the University of California, San Francisco, for valuable discussions on the reconstruction of electron spectra. This work was performed under the auspices of the Alberta Cancer Board.

APPENDIX A: GRADIENTS OF AN OBJECTIVE FUNCTION BASED ON SPECTRAL WEIGHTS

In the calculation of the gradient of the objective function given by Eqs. (9) and (11), we will consider only the cases $m=0$ and $m=1$ which are of practical importance. We estimate the spectrum and its derivative as

$$f(E_n)=\frac{w_n}{\Delta E}, \tag{A1}$$

$$\frac{\partial f(E_n)}{\partial E}=\frac{w_n-w_{n-1}}{\Delta E^2}, \tag{A2}$$

where $\Delta E=E_{n+1/2}-E_{n-1/2}$ is the width of energy step. Then, the zeroth- and first-order stabilizing functions are given by

$$\Omega_0 = \frac{1}{\Delta E}\sum_{n=1}^{N} w_n^2, \tag{A3}$$

$$\Omega_1 = \Omega_0 + \frac{1}{\Delta E^3}\sum_{n=1}^{N} (w_n - w_{n-1})^2. \tag{A4}$$

Substituting Eqs. (A3) and (A4) into Eq. (9) and differentiating we obtain the gradients of the objective function for $m=0$,

$$\frac{\partial \Theta_0}{\partial w_n} = 2\int_0^{z_{\max}} (\overline{D}(z) - D(z)) \cdot d(z,E_n)\, dz + \frac{2\alpha}{\Delta E} w_n, \quad n = 1,...,N, \tag{A5}$$

and for $m=1$,

$$\frac{\partial \Theta_1}{\partial w_n} = \frac{\partial \Theta_0}{\partial w_n} + \frac{2\alpha}{\Delta E^3}(2w_n - w_{n-1} - w_{n+1}), \quad n = 1,...,N. \tag{A6}$$

APPENDIX B: GRADIENTS OF AN OBJECTIVE FUNCTION BASED ON A GAUSSIAN FUNCTION

To calculate the gradient of the least squared objective function $\Phi[f^{\text{sing}}(E)]$ given by Eq. (17) and the analytical singular function $f^{\text{sing}}(E)$ given by Eq. (16), we present the depth-dose distribution $D^{\text{sing}}(z)$ from the analytic function $f^{\text{sing}}(E)$ through the monoenergetic response function $d(z,E)$:

$$D^{\text{sing}}(z) = \int_0^{E_{\max}} d(z,E) f^{\text{sing}}(E)\, dE. \tag{B1}$$

Then, differentiating the objective function $\Phi[f^{\text{sing}}(E)]$ on the parameter we obtain

$$\frac{\partial \Phi}{\partial n} = 2\int_{z_1}^{z_2} (\overline{D}(z) - D^{\text{sing}}(z)) \frac{\partial D^{\text{sing}}(z)}{\partial n} dz, \quad n = \lambda, \sigma, E_0, \tag{B2}$$

where

$$\frac{\partial D^{\text{sing}}(z)}{\partial \lambda} = \frac{1}{\lambda}\int_0^{E_{\max}} d(z,E) f^{\text{sing}}(E)\, dE, \tag{B3}$$

$$\frac{\partial D^{\text{sing}}(z)}{\partial E_0} = \frac{1}{\sigma^2}\int_0^{E_{\max}} d(z,E) f^{\text{sing}}(E)(E - E_0)\, dE, \tag{B4}$$

$$\frac{\partial D^{\text{sing}}(z)}{\partial \sigma} = \frac{1}{\sigma}\int_0^{E_{\max}} d(z,E) f^{\text{sing}}(E)\left(\frac{(E-E_0)^2}{\sigma^2} - 1\right) dE. \tag{B5}$$

[1] D. W. O. Rogers, B. A. Faddegon, G. X. Ding, C. M. Ma, J. We, and T. R. Mackie, "BEAM: A Monte Carlo code to simulate radiotherapy treatment units," Med. Phys. **22**, 503–524 (1995).

[2] J. O. Deasy, P. R. Almond, and M. T. McEllistrem, "Measured electron energy and angular distributions from clinical accelerators," Med. Phys. **23**, 675–684 (1996).

[3] L. Zhengming and D. Jette, "On the possibility of determining an effective energy spectrum of clinical electron beams from percentage depth dose (PDD) data of broad beams," Phys. Med. Biol. **44**, N177–N182 (1999).

[4] B. A. Faddegon and I. Blevis, "Electron spectra derived from depth dose distributions," Med. Phys. **27**, 514–526 (2000).

[5] J. Deng, S. B. Jiang, T. Pawlicki, J. Li, and C.-M. Ma, "Derivation of electron and photon energy spectra from electron beam central axis depth dose curves," Phys. Med. Biol. **46**, 1429–1449 (2001).

[6] J. J. Janssen, E. W. Korevaar, L. J. van Battum, P. R. M. Storchi, and H. Huizenga, "A model to determine the initial phase space of a clinical beam from measured data," Phys. Med. Biol. **46**, 269–286 (2001).

[7] I. Kawrakow, M. Fippel, and K. Friedrich, "3D electron dose calculations using a Voxel based Monte Carlo algorithm (VMC)," Med. Phys. **23**, 445–457 (1996).

[8] A. Chvetsov and G. Sandison, "Semi-analytic electron spectra reconstructed from depth-dose curves," in *Proceedings of the 47th Annual Meeting of the Canadian Organization of Medical Physicists*, Kelowna, BC, Canada, 12–14 July 2001 (Canadian Organization of Medical Physicists, Edmonton, AB, Canada), pp. 88–90.

[9] C. R. Baker, B. Ama'ee, and N. M. Spyrou, "Reconstruction of megavoltage photon spectra by attenuation analysis," Phys. Med. Biol. **40**, 529–542 (1994).

[10] A. Catala, P. Francois, J. Bonnet, and C. Scouarnec, "Reconstruction of 12 MV bremsstrahlung spectra from measured transmission data by direct resolution of the numeric system $AF=T$," Med. Phys. **22**, 3–10 (1995).

[11] G. X. Ding and D. W. O. Rogers, "Energy spectra, angular spread, and dose distributions of electron beams from various accelerators user in radiotherapy," NRC Report, No. PIRS-439 (NRC, Ottawa, March 1995). See also http://www.irs.inms.nrc.ca/inms/irs/papers/PIRS439/pirs439.html.

[12] A. N. Tichonov, "Regularization of incorrectly posed porblems," *Soviet Mathematics, Translation of Doklady Akademii Nauk SSSR* (American Mathematical Society, Providence, Rhode Island, 1963), Vol. 4, pp. 1624–1627.

[13] R. H. Byrd, P. Lu, J. Nocedal, and C. Zhu, "A limited memory algorithm for bound constrained optimization," SIAM J. Sci. Comput. (USA) **16**, 1190–1208 (1995).

[14] C. R. Drumm, "Multidimensional electron-photon transport with standard discrete ordinates codes," Nucl. Sci. Eng. **127**, 1–27 (1997).

[15] C. Borgers, "Complexity of Monte Carlo and deterministic dose-calculation methods," Phys. Med. Biol. **43**, 517–528 (1998).

[16] L. J. Lorence, Jr., J. E. Morel, and G. D. Valdez, "Physics guide to CEPXS: A multigroup coupled electron-photon cross-section generating code," SAND89-1685, Sandia National Laboratories (1989) (available on the Internet: http://www-rsicc.ornl.gov/documents/pdf/ccc/ccc5/c544.pdf).

[17] L. J. Lorence, Jr., J. E. Morel, and G. D. Valdez, "User's guide to CEPXS/ONEDANT: A one-dimentional coupled electron-photon discrete ordinates code package-Version 1.0," SAND89-1661, Sandia National Laboratories (1989) (available on the Internet: http://www-rsicc.ornl.gov/documents/pdf/ccc/ccc5/c544.pdf).

[18] L. J. Lorence, Jr., J. E. Morel, and G. D. Valdez, "Results Guide to CEPXS/ONELD: A One-Dimentional Coupled Electron-Photon Code Package-Version 1.0," SAND89-2211, Sandia National Laboratories (1990) (available on the Internet: http://www-rsicc.ornl.gov/documents/pdf/ccc/ccc5/c544.pdf).

[19] T. A. Germogenova, A. Chvetsov, and A. M. Voloschenko, "Adaptive Positive Nodal Method for Transport Equation," Transp. Theory Stat. Phys. **23**(7), 923–970 (1994).

[20] A. Chvetsov, "Solving the X-Y geometry transport equation by linear discontinuous scheme with consistent flux correction," in *Proceedings Joint International Conference on Mathematical Methods and Supercomputing for Nuclear Applications*, Saratoga Springs, NY, 5–9 October 1997 (American Nuclear Society, La Grange Park, IL, 1997), pp. 1467–1466.

[21] J. E. Morel, "Multigroup Legendre Coefficients for the Diamond Difference Continuous Slowing Down Operator," Nucl. Sci. Eng. **91**, 324 (1985).

[22] H. Neuenschwander, T. R. Mackie, and P. J. Reckwerdt, "MMC-a high-performance Monte Carlo code for electron beam treatment planning," Phys. Med. Biol. **40**, 543–574 (1995).